Effects of Aluminum and Niobium on Impact Properties of Ultra High-Strength TRIP-aided Bainitic Ferrite Steels

Tomohiko HOJO*, Junya KOBAYASHI**, Tomohiro KAJIYAMA** and Koh-ichi SUGIMOTO***

The influence of alloying additions on the impact properties of TRIP-aided bainitic ferrite steel (TBF steel) has been investigated extensively. It has been found that the addition of 0.5 mass% aluminum to a 0.2%C-1.5%Si-1.5%Mn (mass%) TBF steel increases the upper shelf Charpy impact absorbed energy while lowering the fracture appearance transition temperature. This is mainly attributed to the localized stress relaxation due to strain-induced transformation of the fine and carbon enriched retained austenite films. It has also been observed that the addition of both 0.5 mass% aluminum and 0.05 mass% niobium to the steel A improves the impact properties, especially when austempered near the martensite start temperature. This is mainly caused by the refined bainitic ferrite lath structure, stable retained austenite and refined prior austenite grain size achieved by the addition of niobium.
Key Words: TRIP-aided steel; ultra high-strength steel; aluminum; niobium; microstructure; retained austenite; toughness

1. INTRODUCTION

Recently high- and ultra high-strength low alloy TRIP -aided steels associated with transformation induced plasticity (TRIP)[1] have been developed for automotive applications to attain weight reduction and improve the impact safety of vehicles. TRIP-aided steel possesses excellent formability[2-9], hence their use for automotive impact members and centre pillars are expected.

At present, three kinds of TRIP-aided steels, namely TDP (TRIP-aided Dual Phase) steel with polygonal ferrite matrix[2-7], TBF (TRIP-aided Bainitic Ferrite) steel with bainitic ferrite matrix[8] and TAM (TRIP-aided Annealed Martenite) steel with annealed martensite matrix[9] have been developed. As the TBF steel is characterized by the highest tensile strength (780-1470 MPa) and the best toughness in the TRIP-aided steels[10], application as automotive hot-forgings is expected, replacing conventional structural steels. Since it is known that the impact property of TBF steel is greatly affected by the retained austenite characteristics and matrix structure (lath structure and prior austenite grain size), it is necessary to consider whether the addition of alloying element affects impact properties of TBF steel or not. However, the effects of alloying element on the toughness have not been extensively examined although there are very few studies on the TRIP-aided steels[10].

In this study, the effects of addition of aluminum and niobium on impact properties of the TBF steel have been investigated. They have also been related with microstructural features and retained austenite characteristics of the steel.

Received 31. 8. 2012

* Department of Mechanical Engineering

** Graduate Student, Shinshu University

*** Department of Mechanical System Engineering, Shinshu University

2. EXPERIMENTAL PROCEDURE

In this study, three kinds of vacuum melted and hot-forged slabs were prepared. Steel A is the base steel with chemical composition of Fe-0.19%C-1.52%Si -1.51%Mn (mass%). In steel B, aluminum of 0.48 mass% was added to the steel A. Steel C had addition of 0.49 mass% aluminum and 0.05 mass% niobium. Chemical compositions of these three steels are listed in Table 1, with martensite-start temperature (M_S) estimated by the following equation (1)[11].

$$M_S\ (^oC) = 550 - 361 \times (\%C) - 39 \times (\%Mn) - 0 \times (\%Si) + 30 \times (\%Al) - 5 \times (\%Mo) \quad (1)$$

where %C, %Mn, %Si, %Al and %Mo represent contents in mass percent of individual alloying elements, respectively.

Hot-rolling process and heat-treatment diagram are illustrated in Fig. 1 schematically. First, slabs were heated to 1200°C and hot-rolled to 3.2 mm thickness to a finishing rolling temperature of 850°C. Next, the sheet steels were annealed at 950°C for 1200 s in austenitic region and then austempered at 300-475°C for 200 s in

Table 1. Chemical composition (mass%) and estimated martensite-start temperatures (M_S, °C) of steels.

steel	C	Si	Mn	P	S	Al	Nb	N	*Ms*
A	0.19	1.52	1.51	0.015	0.002	0.038	-	0.0013	424
B	0.21	1.48	1.49	0.014	0.002	0.480	-	0.0014	430
C	0.19	1.51	1.50	0.010	0.002	0.480	0.05	0.0012	437

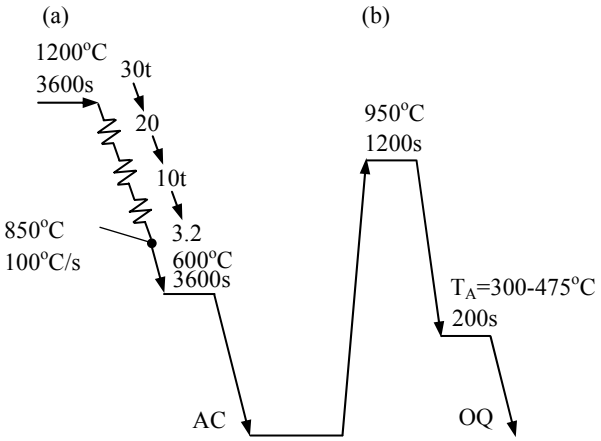

Fig. 1. Hot rolling and heat treatment process of TBF steels.

salt baths to make the TBF steels.

Volume fraction of retained austenite (f_γ, vol%) was quantified from integrated intensity of $(200)_\alpha$, $(211)_\alpha$, $(200)_\gamma$, $(220)_\gamma$ and $(311)_\gamma$ peaks by X-ray diffractometry using Mo-Kα radiation[12]. The carbon concentration (C_γ, mass%) of retained austenite was estimated from the following equation (2). In this case, lattice constant (α_γ, x 10^{-1} nm) was measured from $(200)_\gamma$, $(220)_\gamma$ and $(311)_\gamma$ peaks of Cu-Kα radiation[13].

$$\alpha_\gamma = 3.5780 + 0.0330C_\gamma + 0.00095Mn_\gamma + 0.0056Al_\gamma + 0.0220N_\gamma + 0.0051Nb_\gamma + 0.0031Mo_\gamma \quad (2)$$

where Mn_γ, Al_γ, N_γ, Nb_γ and Mo_γ represent concentrations of individual elements (mass%) in retained austenite. For convenience, bulk compositions of substitutional alloying elements were substituted for these concentrations in this study.

Tensile tests were carried out on a hard type of testing machine at 25°C and at a crosshead speed of 1 mm/min (i.e. strain rate of 8.33 x 10^{-4} /s), using tensile specimens of 20 mm in gauge length, 4 mm in width and 2.5 mm in thickness.

Impact tests were conducted on Charpy impact testing machine at a temperature range between -196 and 150°C. Liquid nitrogen, dry ice and ethanol were used for cooling the specimen. A thermostatic bath was used when the specimen was heated. The specimens were held for 1800 s at the testing temperature before impact testing. Impact properties were evaluated by upper shelf Charpy impact absorbed value (*CIAV*) and fracture appearance transition temperature (*FATT*).

3. RESULTS

3.1. MICROSTRUCTURE AND TENSILE PROPERTIES

Typical scanning electron micrographs and transmission electron micrographs of steels A, B and C are shown in Figs. 2 and 3 respectively. Microstructures of these steels austempered at temperatures above M_S consist of bainitic ferrite matrix with interlath retained austenite films. On the other hand, when austempering treatment is carried out at temperatures below M_S, the lath-like martensite coexists with bainitic ferrite[14]. In this case, volume fraction of the martensite increases with decreasing austempering temperature. Addition of aluminum tends to become finer lath width and retained austenite films in steel B. Further addition of niobium decreases the prior austenite grain size, although a small amount of pro-eutectoid ferrite is formed during cooling after austenitization. In the steel C, NbC is observed in both

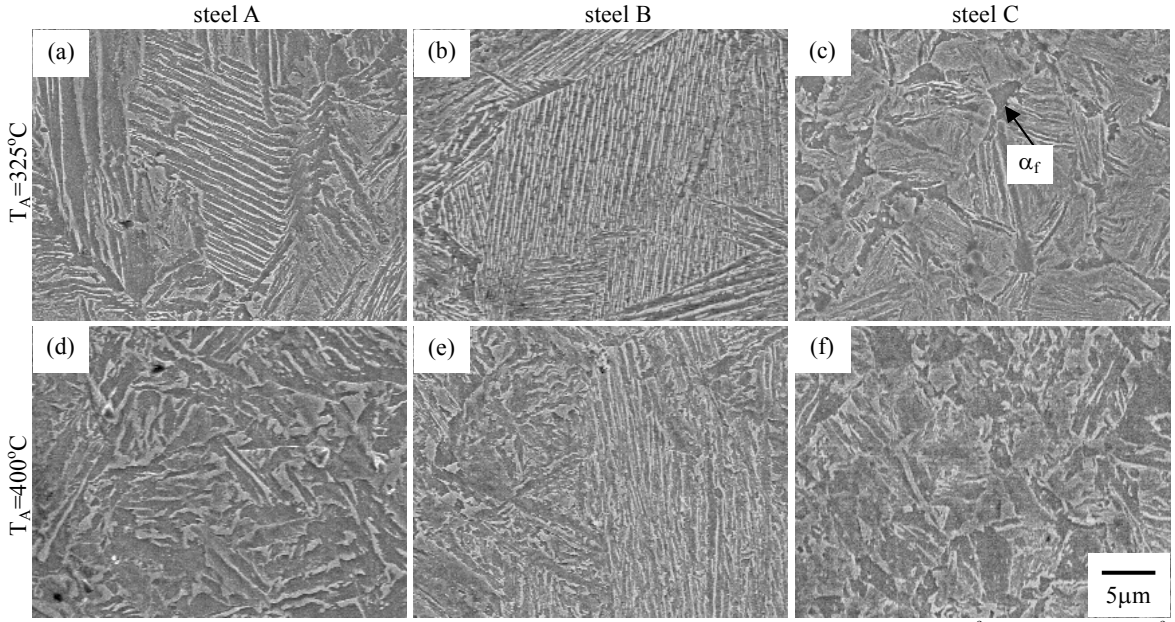

Fig. 2. Scanning electron micrographs of steels (a and d) A, (b and e) B and (c and f) C austempered at (a, b and c) 325 °C or (d, e and f) 400°C, in which α_f is pro-eutectoid ferrite phase.

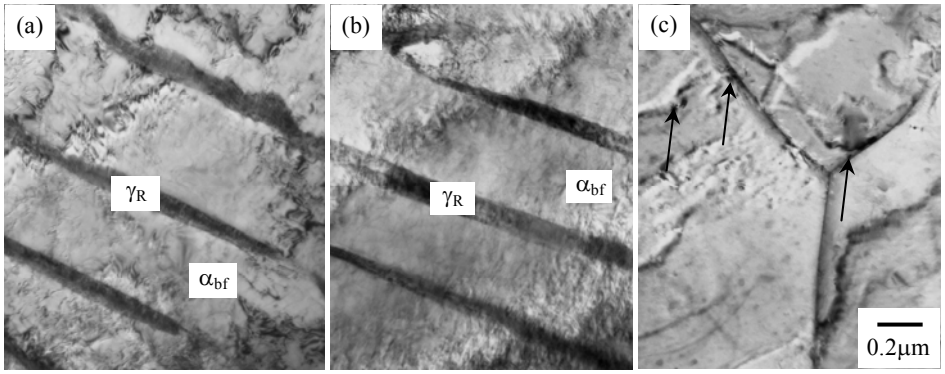

Fig. 3. Transmission electron micrographs of steels (a) A, (b) B and (c) C austempered at 400°C, in which α_{bf} and γ_R represent bainitic ferrite and retained austenite respectively and arrows represent NbC precipitations.

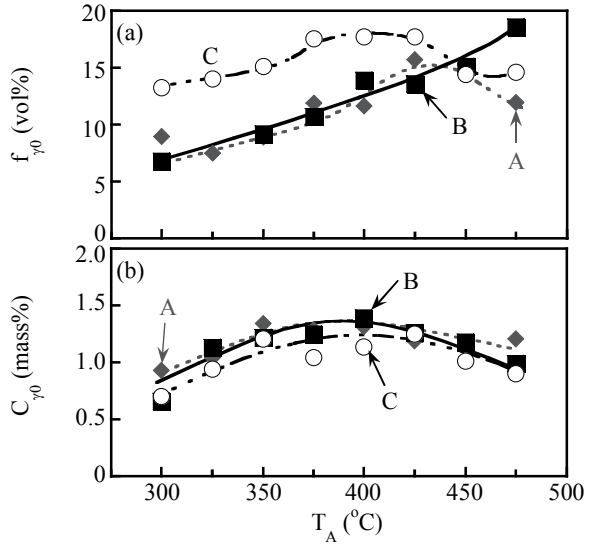

Fig. 4. Variations in (a) initial volume fraction of γ_R ($f_{\gamma 0}$) and (b) initial carbon concentration of γ_R ($C_{\gamma 0}$) as a function of austempering temperature (T_A) in steels A, B and C.

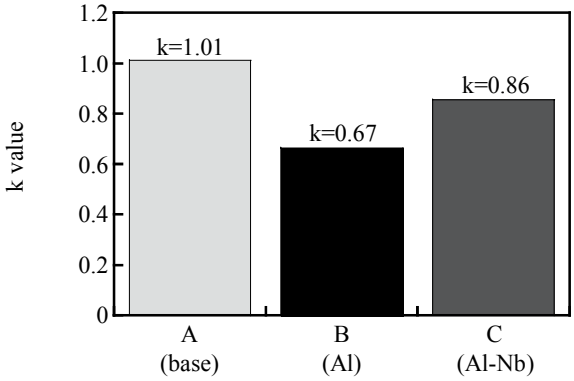

Fig.5. k value of steels A, B and C austempered at 400°C.

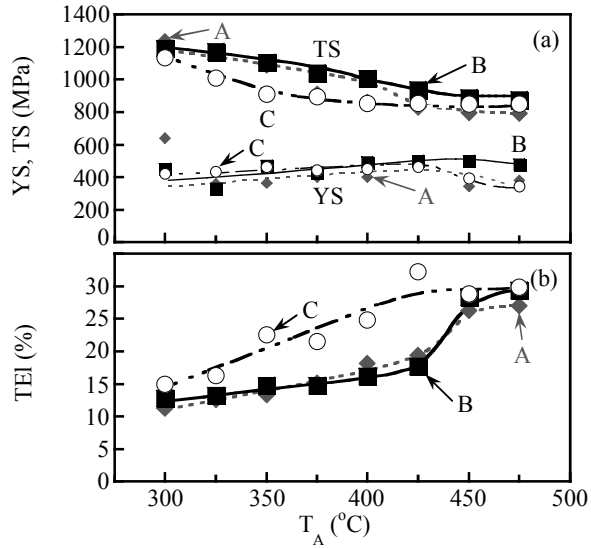

Fig. 6. Variations in (a) tensile strength (*TS*) and yield strngth or 0.2% offset proof stress (*YS*) and (b) total elongation (*TEl*) as a function of austempering temperature (T_A) in steels A, B and C.

the matrix and at grain boundaries (Fig. 3(c)).

The initial volume fraction of retained austenite ($f_{\gamma 0}$) and its carbon concentration ($C_{\gamma 0}$) as a function of austempering temperature of steels A, B and C are shown in Fig. 4. The initial volume fractions of retained austenite in steel A are between 7.5 and 15.7 vol%, and their carbon concentrations are between 0.93 and 1.34 mass% respectively. Initial volume fractions of retained austenite of steel B are hardly changed by aluminum addition, although their carbon concentrations increase a little, compared with those of steel A. On the other hand, combined addition of aluminum and niobium tends to increase the initial volume fraction of retained austenite, with a little decrease in its carbon concentration.

Stability of retained austenite against the strain-induced transformation can be estimated from the carbon concentration of retained austenite. However, the true retained austenite stability should be evaluated by k value which is defined by the following equation (3)[2, 3, 7-9].

$$\log f_\gamma = \log f_{\gamma 0} - k\,\varepsilon \qquad (3)$$

where $f_{\gamma 0}$ and f_γ are initial volume fraction of retained austenite and volume fraction after straining to plastic strain ε in uniaxial tension, respectively. Fig. 5 shows the k values measured in steels A, B and C austempered at 400°C. From Figs. 4(b) and 5, it is found that the lower k value corresponds with higher carbon concentration of retained austenite. So, the high carbon concentration of

retained austenite in Fig. 4(b) means high stability of retained austenite in the present steels.

Fig. 6 shows the tensile properties of steels A, B and C. Tensile strengths (*TS*s) of these steels are between 792 and 1233 MPa and the total elongations (*TEl*s) are between 11.3 and 32.2 % respectively. TBF steels with added aluminum displayed high tensile strength of more than 980 MPa grade at the range of austempering temperature below 400°C compared with steel A. On the other hand, combined additions of aluminum and niobium decrease the tensile strength and increase the total elongation.

3.2. IMPACT PROPERTIES

Fig. 7 shows the typical testing temperature dependence of Charpy impact absorbed value (*CIAV*) of steels A, B and C austempered at 325 and 400°C. Upper shelf *CIAV*s are clearly visible in all steels. It is noted that these *CIAV*s rapidly decrease with decreasing testing temperature for all the steels.

Fig. 8 shows the variations in upper shelf *CIAV* and fracture appearance transition temperature (*FATT*) as a function of austempering temperature (T_A) in steels A, B and C. When the steels are austempered close to their respective M_S, high upper shelf *CIAV*s are obtained. It is clearly indicated in Fig. 8 that the upper shelf *CIAV* is increased and the *FATT* is decreased by aluminum addition and combined addition of aluminum and niobium respectively. It is noteworthy that the *FATT* of steel C is lowered by austempering at region of 375-475°C. Fig. 9 shows the co-relation between the *CIAV* tested at 25°C and *FATT* versus tensile strength (*TS*) for all the steels. When the impact properties of the steels are related to tensile strength, the high upper shelf *CIAV*s and low *FATT*s are achieved in steels B and C.

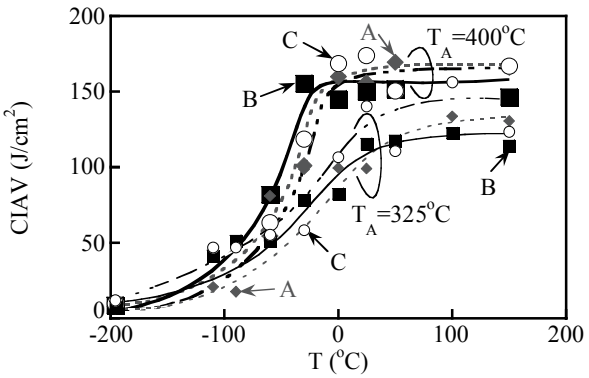

Fig. 7. Charpy impact absorbed value (*CIAV*) - testing temperature (*T*) curves for steels A, B and C austempered at 325°C or 400°C.

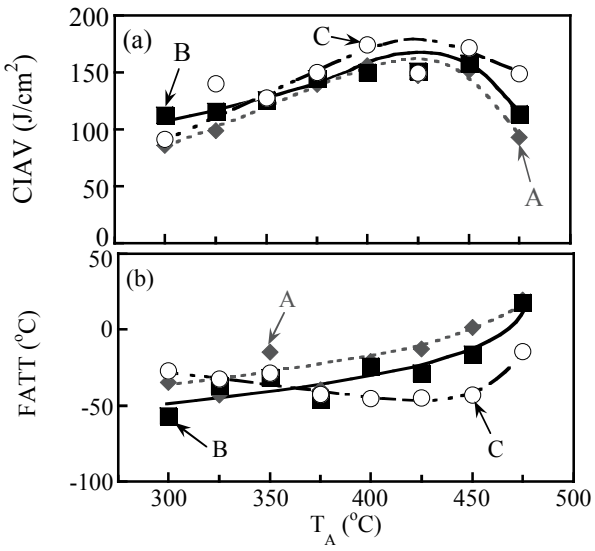

Fig. 8. Variations in (a) Charpy impact absorbed value (*CIAV*) at 25°C and (b) fracture appearance transition temperature (*FATT*) as a function of austempering temperature (T_A) in steels A, B and C.

Figs. 10 and 11 show impact load (*P*)-displacement (δ) curves and crack initiation energy (E_i), crack propagation energy (E_p) and total absorbed energy ($E_t = E_i + E_p$) measured from impact load-displacement curves at 25°C for TBF steels austempered at 325, 400 and 450°C (Fig. 10) and for steels A, B and C austempered at 400°C (Fig. 11). In Fig. 10, the peak of maximum impact load of TBF steel austempered at 450°C is at a larger displacement with lower value than those of transformed at 325 or 400°C. TBF steel austempered at 400°C indicates high E_t and crack propagation energy ratio (E_p / E_t) compared with TBF steels austempering at 325 and 450°C. If aluminum and niobium are both added, peak impact load is decreased compared with steels A and B (Fig. 11(a)). E_t, E_i and E_p of steel B are slightly decreased (Fig. 11(b)). On the other hand, a large difference in E_t, E_i and E_p between steel A and steel C is not observed.

Figs. 12 and 13 show typical scanning electron micrographs of fracture surface and cross sectional area

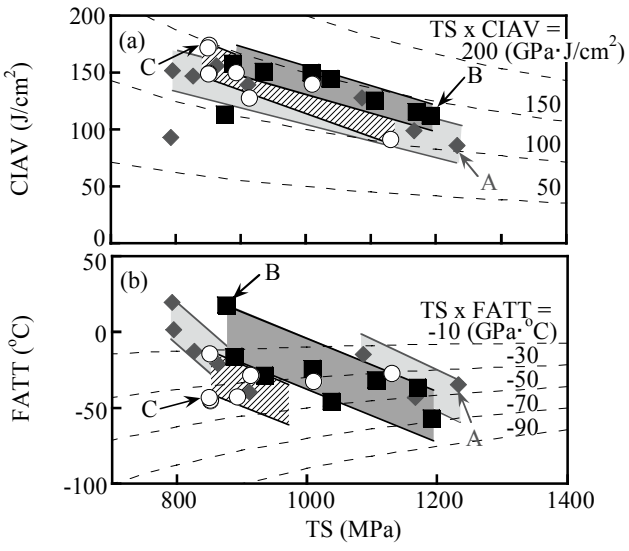

Fig. 9. Relationships of (a) Charpy impact absorbed value (*CIAV*) at 25°C and (b) fracture appearance transition temperature (*FATT*) and tensile strength (*TS*) in steels A, B and C.

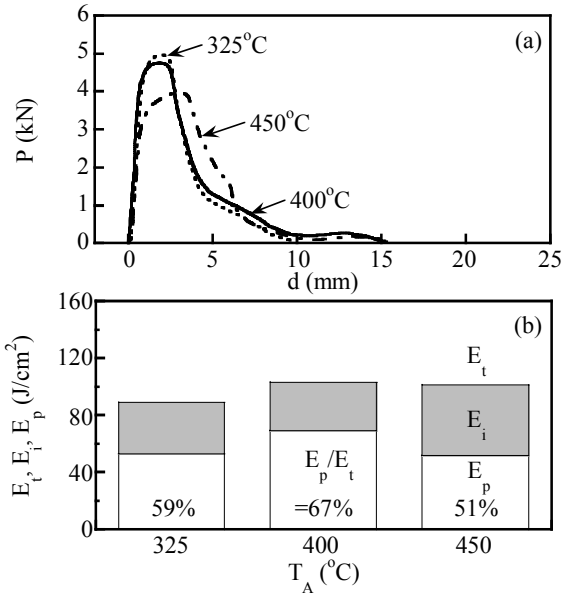

Fig. 10. (a) Impact load (P)-displacement (δ) curves and (b) crack initiation energy (E_i), crack propagation energy (E_p) and total absorbed energy (E_t= E_i+ E_p) measured from impact load-displacement curves at 25°C for steel A austempered at 325, 400 or 450°C.

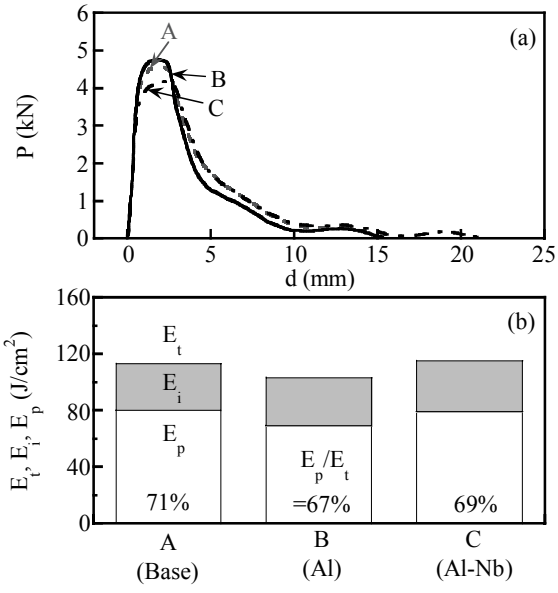

Fig. 11. (a) Impact load (P)-displacement (δ) curves and (b) crack initiation energy (E_i), crack propagation energy (E_p) and total absorbed energy (E_t= E_i+ E_p) measured from impact load-displacement curves at 25°C for steels A, B and C austempered at 400°C.

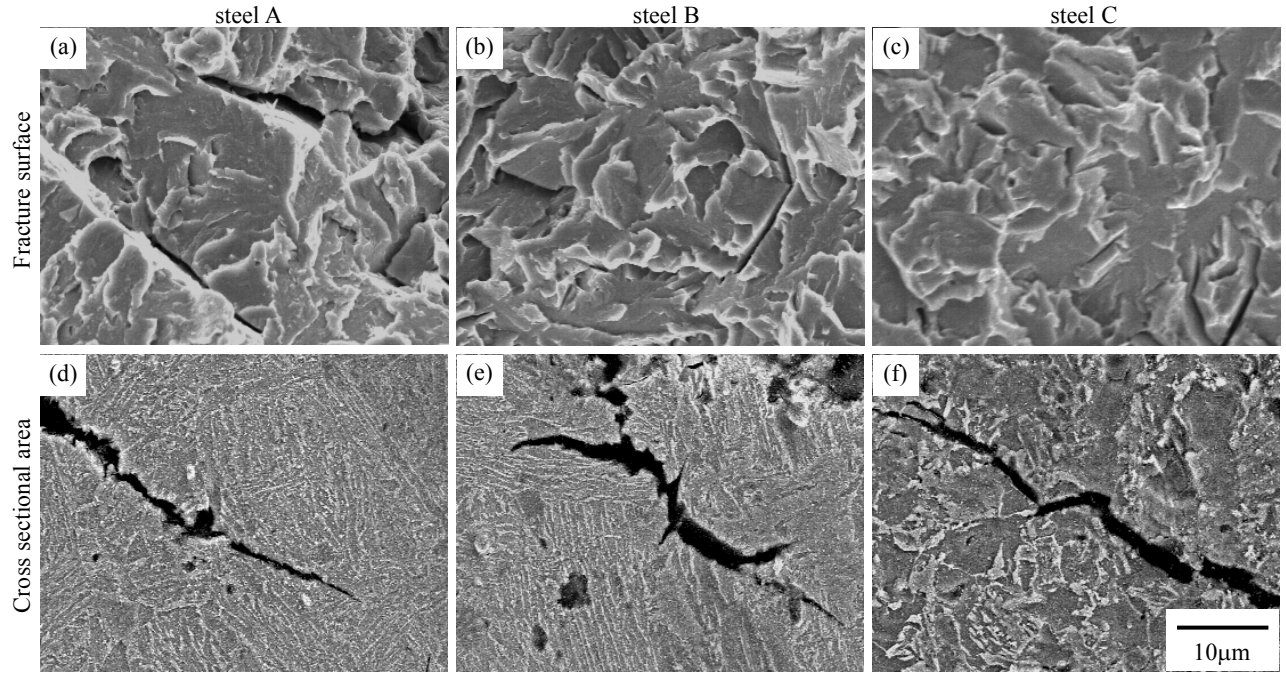

Fig. 12. Scanning electron micrographs of (a, b and c) fracture surface and (d, e and f) cross sectional area near fracture region of steels (a and d) A, (b and e) B and (c and f)C fractured at -196°C. Austempering temperature is 400°C.

near fracture region of steels A, B and C austempered at 400°C tested at -196°C (Fig. 12) and 25°C (Fig. 13). From Fig. 12, it is observed that quasi-cleavage fractures occurred in every TBF steels tested below the *FATT*. In steel C, facet size of quasi-cleavage fracture is decreased, compared with the other steels. The cracks propagate along a bainitic ferrite lath interface in steels A and B. In steel C, the cracks pass across the pro-eutectoid ferrite. In Fig. 13, fracture surface of steels B and C are characterized by deep dimple morphology, although the dimple size is relatively larger than that of steel A.

Initiation of voids is observed at bainitic ferrite lath boundaries in steels A and B. On the other hand, in steel C, the void occurs at pro-eutectoid ferrite interface. Particularly, there are various large voids in steel A

4. DISCUSION

In general, aluminum raises the T_0 (T_0') temperature and increases the carbon concentration of retained austenite with the further consequence of decreasing the volume fraction of retained austenite[15]. On the other hand, niobium decreases the prior austenite grain size compared with steels B and C.

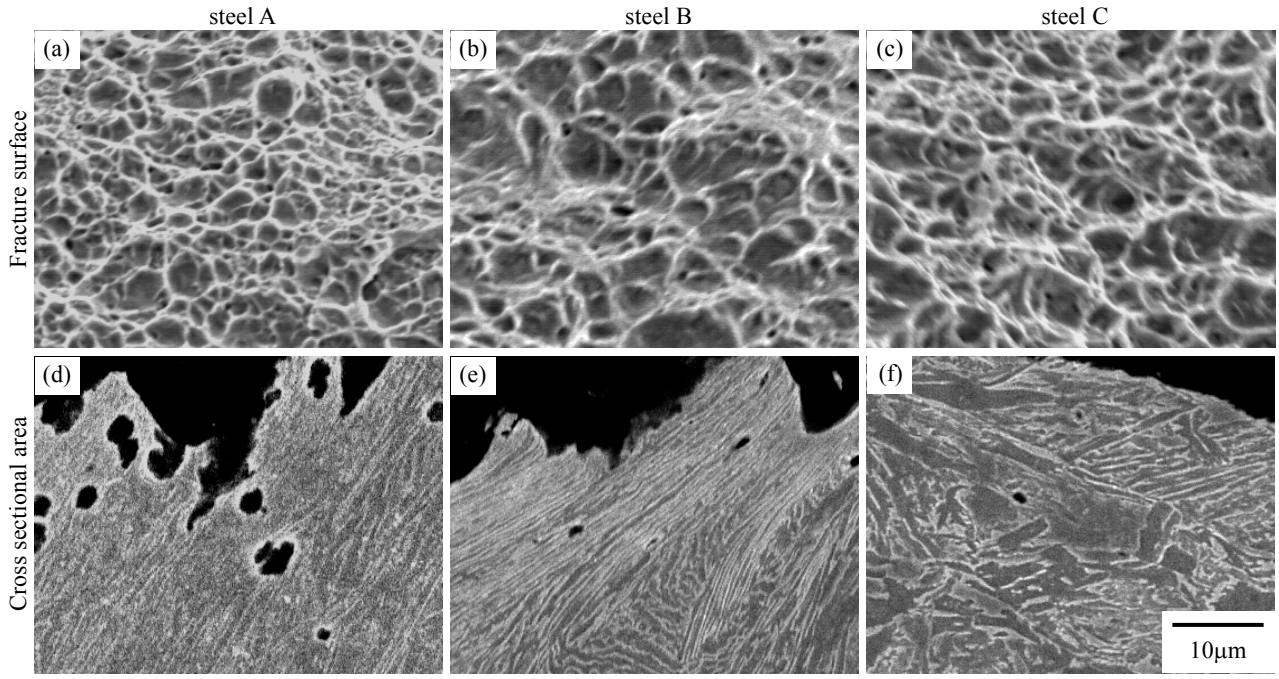

Fig. 13. Scanning electron micrographs of (a, b and c) fracture surface and (d, e and f) cross sectional area near fracture region of steels (a and d) A, (b and e) B and (c and f) C fracture d at 25°C. Austempering temperature is 400°C.

due to the precipitation of NbC at the grain boundary. Niobium tends to lower the carbon concentration of retained austenite[16]. The same tendencies of microstructural change and retained austenite characteristics by addition of aluminum and niobium have been confirmed in this study.

According to the previous study[10], impact properties (i.e. upper shelf *CIAV* and *FATT*) are controlled by the extent of retained austenite, its stability, grain size etc. in TBF steel. If the large amount of stable retained austenite exists in the TBF steel and the size and width of the bainitic ferrite lath are small, the TBF steel can achieve the high upper shelf *CIAV*. In addition, if prior austenite grain is refined with containing few different phases such as dual phase steel, the *FATT* is lowered due to the decreased facet size. Also, the relationship between fracture appearance transition temperature (*FATT*) and unit crack path (*d*) is given by following equation (4)[17].

$$FATT \propto d^{-1/2} \tag{4}$$

In this case, cleavage crack propagation is suppressed by the strain-induced phase transformation of retained austenite because the plastic zone of the crack is much larger than inter particle spacing of retained austenite films[10]. So, the improved impact properties of steels B and C are correlated to the above microstructural properties and retained austenite characteristics.

4.1. EFFECTS OF ALUMINUM ADDITION

In this study, steel B indicates higher *CIAV* at 25°C and lower *FATT* compared with the steel A (Figs. 7, 8 and 9). Fracture surface of TBF steel containing aluminum exhibits larger dimples than that of steel A. It is also observed that initiation and growth of the void at the bainitic ferrite lath boundary is suppressed compared with steel A (Fig. 13). According to Das et al.[18], dimple size of fracture surface at low strain rate became smaller when a large amount of austenite transformed to the martesite in AISI 304LN stainless steel. This result is caused by the suppression of void growth due to martensite transformation. From Figs. 4(b) and 5, it has been indicated that steel B possesses higher carbon concentration of retained austenite and lower *k* value than steel A in this present study. These results mean that it is not easy to transform from retained austenite to martensite in steel B compared with steel A. As shown in Fig. 14, strength-toughness balance (*TS* x *CIAV*) of steels A, B and C is linearly related with initial carbon concentration of retained austenite ($C_{\gamma 0}$). So, it is noted that the improvement of upper shelf *CIAV* of the steel B is caused by the increase in its carbon concentration. This can suppress the initiation and growth of voids at the lath boundary due to the associated localized stress relaxation of the effective strain-induced phase transformation of retained austenite.

Moreover, the microstructure of steel B indicates refined bainitic ferrite lath morphology. It has been reported that void formation is promoted if the second phase particle is large[19] and when the inter particle spacing is small[20]. In steel B, retained austenite films as the second phase are refined in comparison to steel A.

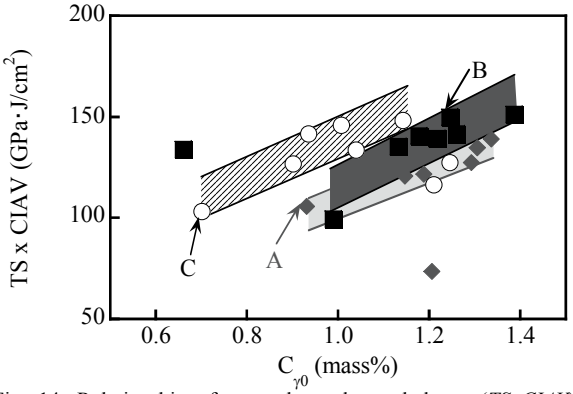

Fig. 14. Relationship of strength-toughness balance (*TS*x*CIAV*) at 25°C and initial carbon concentration of γ_R ($C_{\gamma 0}$) in steels A, B and C.

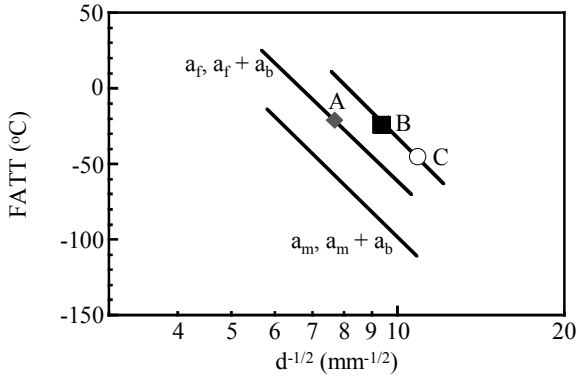

Fig. 15. Relationship between fracture appearance transition temperature (*FATT*) and unit crack path (*d*) in steels A, B and C austempered at 400°C.

This may be also increase the *CIAV* of steel B.

From Fig. 12, the facet size of cleavage fracture surface of steel B is almost the same as that of steel A, and cleavage crack of steel B is propagated along the bainitic ferrite lath boundary. As shown in Figs. 2 and 3, lath width of steel B is decreased and the large amount of refined retained austenite exists along the lath boundaries. So, it is noted that lower *FATT* of steel B is caused by the thin morphology of bainitic ferrite lath structure and more stabilized retained austenite, in the same way as the impact absorbed value.

4.2. EFFECTS OF NIOBIUM ADDITION

Both high *CIAV* at the upper shelf region and low *FATT* have been combined in steel C, especially when austempered between 375 and 450°C. In this case, the microstructure is characterized by fine bainitic ferrite structure with pro-eutectoid ferrite and a large amount of stable retained austenite. From Fig. 13, the dimple size of steel C is large, similar to that of steel B, and few voids are observed at the pro-eutectoid ferrite interface in steel C although void nucleation and growth is suppressed compared with steel A. In Fig. 11(a), displacement of maximum impact load of steel C is larger with lower maximum load than steel A. Generally, the maximum load of this curve corresponds to the initiation point of void nucleation[21]. However, crack initiation energy (E_i), crack propagation energy (E_p) and total absorbed energy (E_t) are almost the same values as those of steel A (resultantly E_p / E_t is almost same value) (Fig. 11(b)). So Fig. 11 suggests that steel C suppresses the void initiation until large deformation region during impact test. As mentioned above, localized stress relaxation due to the strain-induced martensite transformation suppresses the void nucleation and growth. Steel C exhibits excellent retained austenite characteristics compared with steel A (Which may be mainly caused by the aluminum addition). It is likely that high upper shelf *CIAV* of steel C is due to the fine and a large amount of stable retained austenite. In this case, pro-eutectoid ferrite may not influence the upper shelf *CIAV* although it decreases the tensile strength.

From Fig. 12, the facet size observed on the fracture surface of steel C is smaller than that of other steels, corresponding to the size of prior austenite grain. This fine prior austenite grain size is obtained by the precipitation of NbC. In addition, the crack of steel C is propagated not along the lath boundary but across the pro-eutectoid ferrite. Fig. 15 shows the relationship between fracture appearance transition temperature (*FATT*) and unit crack path (*d*) in steels A, B and C austempered at 400°C. The results of ferrite-bainaite or bainitic and martensite-bainite or martensitic steels which do not include the retained austenite are also shown in this figure[17]. The *FATT* of TBF steel is lowered with decreasing unit crack path. So, it is noted that low *FATT* of steel C is principally caused by the refined prior austenite grain size and mixed fine morphology of the grain. Also, the stabilized fine retained austenite suppresses the initiation and growth of cleavage crack formation. Therefore steel C exhibits lower the *FATT*.

5. CONCLUSIONS

The effects of aluminum and niobium on impact properties of TBF steels with tensile strength more than 980 MPa have been investigated. Main results are summarized as follows.

(1) Aluminum addition of 0.5 mass% to the steel A increases upper shelf Charpy impact absorbed value and lowers the fracture appearance transition temperature. The improvement of the impact properties are associated with localized stress relaxation due to the strain-induced transformation of the fine and carbon enriched retained austenite films.

(2) Combined additions of 0.5 mass% aluminum and

0.05 mass% niobium to the steel A improves the impact properties, especially when austempered at temperatures between 375 and 450^{o}C. This is mainly caused by not only the refined bainitic ferrite matrix, retained austenite films and prior austenite grain size but also large amount of stable retained austenite by aluminum and niobium combined addition.

ACKNOWLEDGEMENTS

The authors gratefully acknowledge financial support by the Grant-in-Aid for Scientific Research (B), The Ministry of Education, Science, Sports and Culture, Japan (No.2008-20360311).

REFERENCES

1) V. F. Zackay, E. R. Parker, D. Fahr and R. Bush: Trans. Am. Soc. Met., 60 (1967)252-259
2) K. Sugimoto, N. Usui, M. Kobayashi and S. Hashimoto: ISIJ Int., 32 (1992)1311-1318
3) K. Sugimoto, M. Kobayashi and S. Hashimoto: Metall. Trans. A, 23A (1992)3085-3091
4) O. Matsumura, Y. Sakuma, Y. Ishii and J. Zhao: ISIJ Int., 32 (1992)1110-1116
5) Z. Hanzaki, P. D. Hodgson and S. Yue: ISIJ Int., 35 (1995)79-85
6) A. Nagasaka, K. Sugimoto, M. Kobayashi, Y. Kobayashi and S. Hashimoto: Tetsu-to-Hagane, 87 (2001)607-612
7) K. Sugimoto, A. Nagasaka, M. Kobayashi and S. Hashimoto: ISIJ Int., 39 (1999)56-63
8) K. Sugimoto, J. Sakaguchi, T. Iida and T. Kashima: ISIJ Int., 40 (2000)920-926
9) K. Sugimoto, A. Kanda, R. Kikuchi, S. Hashimoto, T. Kashima and S. Ikeda: ISIJ Int., 42 (2002)910-915
10) S. Song, K. Sugimoto, M. Kobayashi,H. Matsubara and T. Kashima: Tetsu-to-Hagane, 86 (2000)563-569
11) I. Tamura: Steel Material Study on the Strength, Nikkan Kogyo Shinbun Ltd., Tokyo, (1970)40
12) H. Maruyama: J. Jpn. Soc. Heat Treat., 17 (1977)198-204
13) D. J. Dyson and B. Holmes: J. Iron Steel Inst., 208 (1970)469-474
14) M. Murata, J. Kobayashi and K. Sugimoto: Tetsu-to-Hagane, 96, (2010)84-92
15) K. Sugimoto, B. Yu, Y. Mukai and S. Ikeda: ISIJ Int., 45 (2005)1194-1200
16) W. Bleck, A. Frehn and J. Ohlert: Proc. of Int. Sympo. Niobium 2001, TMS, PA, (2001)727-752
17) H. Ohtani, F. Terasaki and T. Kunitake: Tetsu-to-Hagane, 58 (1972)434-451
18) A. Das and S. Tarafder: Int. J. Plast., 25 (2009)2222-2247
19) J. J. Gurland and J. Plateau: Trans. ASM., 56 (1963)442-454
20) T. Inoue and S. Kinoshita: J. Jpn. Soc. Technol. Plast., 14 (1973)291-297
21) H. Nakazawa: Manual of Test for Metallic Material, Japanese Standards Association, Tokyo, (1987)82